Cascading Optical Negative Index Metamaterials

Alexander V. Kildishev and Uday K. Chettiar

Birck Nanotechnology Center, School of Electrical and Computer Engineering
Purdue University, IN 47907 USA (e-mail: a.v.kildishev@ieee.org)

Abstract **—** We use a spatial harmonic analysis (SHA) method to homogenize optical metamaterials with a negative refractive index; the method provides a more general approach than other methods for estimating the effective index of materials arranged of cascaded elementary layers. The approach is validated for a single layer and a triple layer two dimensional metal grating.

Index Terms **—** Negative Index Metamaterial, Spatial Harmonic Analysis (SHA), Homogenization.

I. INTRODUCTION

The refractive index ($n = n' + in''$) is the key parameter in the interaction of light with matter. While n' has generally been considered to be positive, the condition $n' < 0$ does not violate any fundamental physical law, and materials with negative index have some remarkable properties. Such materials are called negative-index materials (NIMs), and in these materials the phase velocity is directed against the flow of energy. There are no known naturally-occurring optical NIMs. Optical properties of such media have been considered in early papers by Mandel'shtam [1] and Veselago [2]. Proof-of-principle experiments [3] have shown that artificially designed materials (metamaterials) consisting of split ring resonators (SRRs) and metal wires can act as NIMs at microwave wavelengths. NIMs drew a large amount of attention after Pendry predicted that NIMs can act as a superlens allowing for an imaging resolution which is limited not by the wavelength but rather by material quality [4].

A. Homogenization of an Elementary Layer

A possible approach to designing negative index materials is a periodic array of elementary coupled metal-dielectric resonators. This work takes a closer look at approaches which simultaneously provide fast calculation of the field inside a given metamaterial arranged of elementary periodic layers and calculation of its effective parameters.

First we review an established approach to homogenization of a thin layer of NIM. For a given monochromatic incident light, it is possible to measure the complex reflectance and transmittance coefficients (r and t) and then unambiguously retrieve the refractive index of the NIM sample. This effective parameter can be conveniently obtained from the characteristic matrix of a homogeneous film at normal incidence [5].

Here we consider an effective layer of NIM over a homogeneous thick substrate with a refractive index n_2, as shown in Fig. 1. The conservation of the tangential electric and magnetic fields at the first interface gives the standard boundary conditions (BCs), $H_0 = H_1$, $E_0 = E_1$. Then, using the definitions of the complex reflection and transmission coefficients ($\overline{r}_0 = E_{0,r}/E_i$, $\overline{t}_1 = E_{1,t}/E_i$, and $\overline{r}_1 = E_{1,r}/E_i$), we have

$$\mathbf{V}\begin{pmatrix}1\\ \overline{r}_0\end{pmatrix} = \mathbf{D}_1\mathbf{V}\begin{pmatrix}\overline{t}_1\\ \overline{r}_1\end{pmatrix}, \tag{1}$$

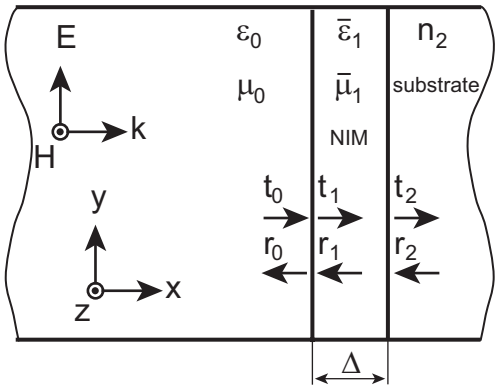

Fig. 1. Simplified approach to the homogenization of a thin equivalent layer of NIM on top of a thick substrate with a refractive index n_2. The equivalent layer is characterized by the effective permittivity and permeability. Note that $r_2 = 0$, provided that the layer is not illuminated.

where $\mathbf{V}$ is a rotation matrix.

$$\mathbf{V} = \begin{pmatrix} 1 & -1 \\ 1 & 1 \end{pmatrix}, \tag{2}$$

and

$$\mathbf{D}_1 = \begin{pmatrix} \overline{\eta}_1^{-1} & 0 \\ 0 & 1 \end{pmatrix}, \tag{3}$$

where $\overline{\eta}_1 = \sqrt{\overline{\mu}_1 / \overline{\varepsilon}_1}$ is the effective impedance of the NIM layer with effective permeability $\overline{\mu}_1$ and effective permittivity $\overline{\varepsilon}_1$.

Then, using the scaled thickness of the layer, $\delta_1 = 2\pi \Delta_1 / \lambda$, with the transport matrix

$$\mathbf{A}_1 = \begin{pmatrix} e^{-\iota \overline{n}_1 \delta_1} & 0 \\ 0 & e^{\iota \overline{n}_1 \delta_1} \end{pmatrix}, \tag{4}$$

i.e., backpropagating $\overline{r}_1$ and propagating $\overline{t}_1$ up to the second interface we arrive at the equation

$$\mathbf{D}_1 \mathbf{V} \mathbf{A}_1^{-1} \begin{pmatrix} \overline{t}_1 \\ \overline{r}_1 \end{pmatrix} = \begin{pmatrix} n_2 \overline{t}_2 \\ \overline{t}_2 \end{pmatrix}. \tag{5}$$

Combining (1) and (5) gives the following form

$$\begin{pmatrix} 1 - \overline{r}_0 \\ 1 + \overline{r}_0 \end{pmatrix} = \mathbf{D}_1 \mathbf{V} \mathbf{A}_1 \mathbf{V}^{-1} \mathbf{D}_1^{-1} \begin{pmatrix} n_2 \overline{t}_2 \\ \overline{t}_2 \end{pmatrix}. \tag{6}$$

From the above we have

$$\mathbf{V}^{-1} \mathbf{D}_1^{-1} \begin{pmatrix} 1 - \overline{r}_0 \\ 1 + \overline{r}_0 \end{pmatrix} = \mathbf{A}_1 \mathbf{V}^{-1} \mathbf{D}_1^{-1} \begin{pmatrix} n_2 \overline{t}_2 \\ \overline{t}_2 \end{pmatrix} \tag{7}$$

or

$$\begin{pmatrix} \dfrac{1 + \overline{r}_0 + (1 - \overline{r}_0)\overline{\eta}_1}{\overline{t}_2 (1 + n_2 \overline{\eta}_1)} \\ \dfrac{1 + \overline{r}_0 - (1 - \overline{r}_0)\overline{\eta}_1}{\overline{t}_2 (1 - n_2 \overline{\eta}_1)} \end{pmatrix} = \begin{pmatrix} e^{-\iota \overline{n}_1 \delta_1} \\ e^{\iota \overline{n}_1 \delta_1} \end{pmatrix}. \tag{8}$$

Then, multiplying the components of each vector from both sides we arrive at

$$\overline{\eta}_1 = \pm \sqrt{\frac{(1 + \overline{r}_0)^2 - \overline{t}_2^2}{(1 - \overline{r}_0)^2 - \overline{t}_2^2 n_2^2}}, \tag{9}$$

while summing up the components and using (9) gives

$$\cos \overline{n}_1 \delta_1 = \frac{1 - \overline{r}_0^2 + n_2 \overline{t}_2^2}{\left[(1 + \overline{r}_0) n_2 + 1 - \overline{r}_0\right] \overline{t}_2}. \tag{10}$$

Equation (6) can be written in another manner as

$$\mathbf{Q}_0 = \mathbf{M}_1 \mathbf{Q}_2, \tag{11}$$

using $\mathbf{Q}_0 = \begin{pmatrix} t_0 \\ r_0 \end{pmatrix}$, $\mathbf{Q}_2 = \begin{pmatrix} t_2 \\ r_2 \end{pmatrix}$, and $\mathbf{M}_1 = \mathbf{S}_1 \mathbf{A}_1 \mathbf{S}_1^{-1}$, where $\mathbf{S}_1$ is the symmetric matrix, $\mathbf{S}_1 = \mathbf{V}^{-1} \mathbf{D}_1 \mathbf{V}$. Note that for a single layer on a substrate, $r_2 = 0$ and t_0 is the incident field.

B. Nomenclature of Matrix Functions

To simplify the notations (and further programming), nomenclature for matrix functions is defined in parallel with direct matrix notation. First, we introduce a general 2×2 matrix partitioning function ($\mathbf{w}$) with partitions comprised of four different $\widehat{m} \times \widehat{m}$ square matrices ($w^{0,0}, w^{0,1}, w^{1,0}, w^{1,1}$):

$$\mathbf{w}\left(w^{0,0}, w^{0,1}, w^{1,0}, w^{1,1}\right) = \left(\begin{array}{c|c} w^{0,0} & w^{0,1} \\ \hline w^{1,0} & w^{1,1} \end{array}\right). \tag{12}$$

Second, using (12) we add a partitioning function ($\mathbf{s}$) for arranging four bi-diagonally symmetric partitions combined of two $\widehat{m} \times \widehat{m}$ matrices (s_0 and s_1):

$$\mathbf{s}(s_0, s_1) = \mathbf{w}(s_0, s_1, s_1, s_0) = \left(\begin{array}{c|c} s_0 & s_1 \\ \hline s_1 & s_0 \end{array}\right). \tag{13}$$

Then, using (12) and a $\widehat{m} \times \widehat{m}$ null matrix (o) we suggest to define another function ($\mathbf{d}$) for making a diagonally partitioned matrix of two $\widehat{m} \times \widehat{m}$ matrices (b_0 and b_1) as

$$\mathbf{d}(b_0, b_1) = \mathbf{w}(b_0, \mathrm{o}, \mathrm{o}, b_1) = \left(\begin{array}{c|c} b_0 & \mathrm{o} \\ \hline \mathrm{o} & b_1 \end{array}\right). \tag{14}$$

In addition, the following constant rotation matrix arranged of $2\widehat{m} \times 2\widehat{m}$ identity matrices (i) is used

$$\mathbf{i} = \mathbf{w}(\mathrm{i}, -\mathrm{i}, \mathrm{i}, \mathrm{i}) = \left(\begin{array}{c|c} \mathrm{i} & -\mathrm{i} \\ \hline \mathrm{i} & \mathrm{i} \end{array}\right). \tag{15}$$

Finally, a stacking function ($\mathbf{c}$) is defined for a stacked vector made of two equal vectors (v_1, v_2) with $\hat{m}$ components as

$$\mathbf{c}(v_1, v_2) = \begin{pmatrix} v_1 \\ v_2 \end{pmatrix}. \tag{16}$$

Thus for example, (2)-(4) and (11) can be rewritten using (12)-(16) for $\hat{m} = 1$ as

$$\mathbf{Q}_0 = \mathbf{c}(t_0, r_0),\ \mathbf{Q}_2 = \mathbf{c}(t_2, r_2), \tag{17}$$

$$\mathbf{A}_1 = \mathbf{d}\left(e^{-\iota\overline{n}_1\delta}, e^{\iota\overline{n}_1\delta}\right),\ \mathbf{D}_1 = \mathbf{d}\left(\eta_1^{-1}, 1\right),\ \mathbf{V} = \mathbf{i}. \tag{18}$$

C. Basics of SHA in Cascaded NIM Layers

Equations (9) and (10) provide an easy approach to the characterization of thin metamaterials. With this simple assumption it is thought that a cascaded bulk material can be arranged using a stack of q equivalent layers with an effective transformation matrix $\mathbf{M}^q = \mathbf{S}\mathbf{A}^q\mathbf{S}^{-1}$. In general, this straightforward approach assumes that the spatial harmonics of each layer interact only with the same harmonics of other layers in the stack. In essence, this loose assumption ignores any transformation of a given incident harmonic into the spatial harmonics of different order, which are either reflected or transmitted. To illustrate this issue, consider another approach to obtaining effective parameters of a multilayer NIM arranged of thin infinite elementary layers with periodic distribution of elementary materials. Essentially, the enhanced method follows the recipe for a classical case of stratified media (see for example, [6]-[11]).

We note that a variety of rigorous algorithms have been based on SHA for diffraction gratings. After the publications of Burckhardt [7], Kaspar [8], and Knop [9], a very similar method was introduced by Moharam and Gaylord [10]-[12]. Analytical approaches to the problem were shown by Botten and McPhedran [13]-[15]. An alternative to Botten's method was discussed by Tayeb and Petit [16]-[18]. Due to space constrains, here we only give a brief list of early publication; a larger review will be published elsewhere.

We start with monochromatic Maxwell's equations $\nabla\times\vec{E} = \iota\omega\vec{B}$, $\nabla\times\vec{H} = -\iota\omega\vec{D}$ arriving at

$$\begin{aligned} k^2n^2\vec{H} &= \nabla\times\nabla\times\vec{H} - \nabla\ln\varepsilon\times\nabla\times\vec{H}, \\ k^2n^2\vec{E} &= \nabla\times\nabla\times\vec{E} - \nabla\ln\mu\times\nabla\times\vec{E}. \end{aligned} \tag{19}$$

In addition, using $\nabla\cdot\vec{B} = 0$ and $\nabla\cdot\vec{D} = 0$ we have

$$\begin{aligned} \nabla\cdot\vec{H} &= -\nabla\ln\mu\cdot\vec{H}, \\ \nabla\cdot\vec{E} &= -\nabla\ln\varepsilon\cdot\vec{E}, \end{aligned} \tag{20}$$

and finally

$$\begin{aligned} k^2n^2\vec{H} + \nabla^2\vec{H} &= -\nabla\left(\nabla\ln\mu\cdot\vec{H}\right) \\ &\quad -\nabla\ln\varepsilon\times\nabla\times\vec{H}, \\ k^2n^2\vec{E} + \nabla^2\vec{E} &= -\nabla\left(\nabla\ln\varepsilon\cdot\vec{E}\right) \\ &\quad -\nabla\ln\mu\times\nabla\times\vec{E}. \end{aligned} \tag{21}$$

D. Bloch-Floquet Waves in Cascaded 2D Layers

A simpler 2D example is used here to illustrate the approach because derivations for the spatial harmonic analysis (SHA) in 2D are less difficult. Consider a single period (l) of an infinite interface of a free-space domain with the domain of a material characterized by a set of step-wise continuous permittivity values ($\varepsilon_{1,1}$, $\varepsilon_{2,1}$, …), as shown in Fig. 2a.

Provided that a TM ($\vec{H} = \hat{\mathbf{z}}\cdot h$) boundary-value problem is taken, then only the tangential components of the H and E field distributions over l are required in this case. A local coordinate system is introduced, with a unit normal ($\hat{\mathbf{x}}$), a unit transverse vector ($\hat{\mathbf{z}}$) and a tangent unit vector ($\hat{\mathbf{y}}$). Then, consider two scalar fields (h and d) as the distribution of the transverse magnetic field ($h = \hat{\mathbf{z}}\cdot\vec{H}$) over l and the distribution the electric field ($d = \varepsilon\hat{\mathbf{y}}\cdot\vec{E}$). A monochromatic Maxwell equation $\hat{\mathbf{y}}\cdot(\nabla h\times\hat{\mathbf{z}}) = -\iota\omega d$ couples the fields

$$d = (i\omega)^{-1}h', \tag{22}$$

where the normal derivative of h is denoted $h' = \hat{\mathbf{x}}\cdot\nabla h$.

The core of any SHA approach is the transformation of the fields from a physical space to spatial spectral space using available proper functions (g^m). Provided that h and g^m are sets of discrete values obtained at a uniform grid on l, these sets are considered as two vec-

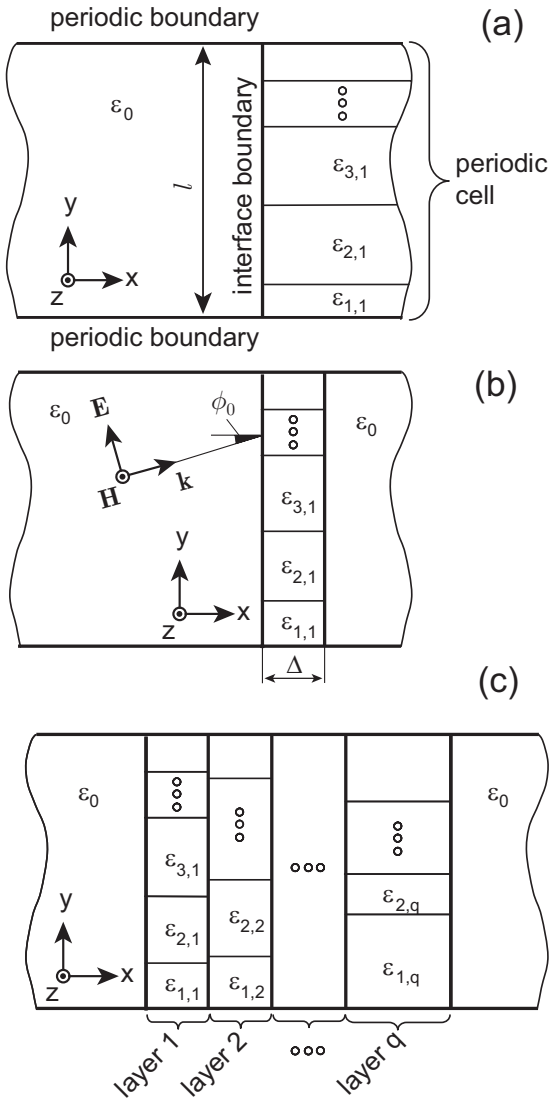

Fig. 2. (a) Interface of an elementary layer of NIM with free space; (b) an isolated elementary layer; (c) a cascaded multilayer NIM.

tors (h and g^m). The sum $\sum_{p=-p_{\max}}^{p_{\max}} g_p^{\nu *} g_p^m$ is considered here as a scalar product of two vectors $\left(g^\nu, g^m\right)_l$, where p is a point of the grid on l arranged of $\hat{p} = 2p_{\max} + 1$ points. Note that the proper functions g^m are orthonormal on l, i.e. $\left(g^\nu, g^m\right)_l = \delta(m-\nu)$.

Let us isolate the first elementary layer, for example, as shown in Fig. 2b. The magnetic field is defined by $h_1 = \sum_{m=-\infty}^{\infty} g_t^m c_{t,1}^m + g_r^m c_{r,1}^m$, where g_t^m and g_r^m are transmitted and reflected elementary fields of order m. In essence, the field h_1 is decomposed into elementary fields (the Bloch-Floquet waves), which are orthonormal on l. In a truncated approximation, $|m| \le m_{\max}$, the vectors g^m can form a $\hat{p} \times \hat{m}$ matrix g, $\hat{m} = 2m_{\max} + 1$ and the complex magnitudes of the reflected and transmitted fields ($c_{r,1}^m$ and $c_{t,1}^m$) can be taken as the components of two different $\hat{m}$ - dimensional vectors $c_{r,1}$ and $c_{t,1}$. Then, the magnetic field in matrix form is defined by $h_1 = g_{t,1} c_{t,1} + g_{r,1} c_{r,1}$.

The Bloch-Floquet theorem allows for the separation of variables, $g_t = v_1 u_1$ and $g_r = v_1 u_1^{-1}$, where u is an $\hat{m} \times \hat{m}$ matrix exponential, $u_1 = \exp \imath k_{x,1} k x$, of a proper values matrix, $k_{x,1}^m$; and v_1 is a $\hat{p} \times \hat{m}$ matrix constructed of orthogonal vectors v_1^m. For the free-space case, indices in u, v, and k_x^m are dropped, and the proper functions u are defined through $k_x^m = \sqrt{1 - \left(k_y^m\right)^2}$, where $k_y^m = m\lambda l^{-1} + \sin\phi_0$ and ϕ_0 is the angle of incidence (shown in Fig. 2b). The wavefront $v^m = \hat{p}^{-1/2} \exp \imath k_y^m k y$ is just an orthonormal Fourier component of the m^{th} order.

1) Eigenvalue Problem

To obtain both $k_{x,1}$ and a_1 for a given elementary layer, where the permittivity of elementary materials (a piece-wise continuous function ε_1) is periodic in the y direction but constant in the x direction, it is necessary to attain an eigenvalue problem formulation. In this case,

$$k^2 \varepsilon_1 h_1 + \nabla^2 h_1 - f_1 \partial_y h_1 = 0\,, \tag{23}$$

where f is the logarithmic derivative, $f_1 = \partial_y \ln \varepsilon_1$, ε_1 and ε_1^{-1} are $\hat{p} \times \hat{p}$ diagonal matrices, and k^2 is a scalar.

The above equation can then be rewritten using $h_1 = v_1\left(u_1 c_{t,1} - u_1^{-1} c_{r,1}\right)$. Next, introducing a_1 as an $\hat{m} \times \hat{m}$ matrix mapping an orthogonal basis v_1 into the free-space basis v, ($v_1 = v a_1$), substituting $\imath\left(v^{-1} f_1 v\right) k_y$ with $\imath\left(k_y v^{-1}\varepsilon_1 v - v^{-1}\varepsilon_1 v k_y\right) \imath v^{-1}\varepsilon_1^{-1} v k_y$ and using γ_1 for $v^{-1}\varepsilon_1 v$, $\tilde{\gamma}_1$ for $v^{-1}\varepsilon_1^{-1} v$ and i for the $\hat{m} \times \hat{m}$ identity matrix, (23) is further simplified as

$$a_1 k_{x,1}^2 a_1^{-1} = \gamma_1\left(\mathrm{i} - k_y \tilde{\gamma}_1 k_y\right). \tag{24}$$

The transform a_1 is required because in contrast with the free-space case, each wavefront v_1^m in an elementary inhomogeneous layer is not a single Fourier com-

ponent anymore; however, as a 'physical function'♦ it still can be expressed as a superposition of Fourier components. Note that equation (24) is written in an eigenvalue form since $k_{x,1}^2$ is a diagonal matrix. The equation can be solved either numerically or analytically for both $k_{x,1}^2$ and a_1, provided that γ_1 and k_y are known.

2) Mixed Boundary-Value Problem

Transverse field continuity together with the conservation of the tangential electric field on l gives the standard boundary conditions (BCs), $h_0 = h_1$, $\varepsilon_1 h_0' = h_1'$, where the pairs h, h' represent the magnetic field and its normal derivative just before and after the interface; ε_1 are the values of permittivity at the collocation points on l.

After using the definitions of the fields $h_0 = v\left(uc_{t,0} - u^{-1}c_{r,0}\right)$, $h_1 = va_1\left(u_1c_{t,1} - u_1^{-1}c_{r,1}\right)$ and taking the normal derivatives, a spectral form of the BC is

$$c_0 = s_1 c_1 . \tag{25}$$

Here,

$c_0 = \mathbf{d}\left(u, u^{-1}\right)\mathbf{c}\left(c_{t,0}, c_{r,0}\right)$, $c_1 = \mathbf{d}\left(u_1, u_1^{-1}\right)\mathbf{c}\left(c_{t,1}, c_{r,1}\right)$, and $s_1 = \mathbf{i}^{-1}\mathbf{d}\left(a_1, k_x^{-1}\gamma_1^{-1}a_1k_{x,1}\right)\mathbf{i}$.

At the second interface (as shown in Fig. 2b), the equation for the elementary layer is given by

$$b_1c_1 = s_1^{-1}c_2 , \tag{26}$$

where $b_1 = \mathbf{d}\left(\beta_1, \beta_1^{-1}\right)$; the matrix exponential $\beta_1 = \exp \iota k_{x,1}\delta_1$ adjusts the phases for the scaled thickness of the layer ($\delta_1 = 2\pi\,\Delta_1/\lambda$).

Combining (25) and (26) gives the following form

$$c_0 = s_1b_1^{-1}s_1^{-1}c_2 . \tag{27}$$

Since k_x is given as a common matrix for all layers, a possible alternative is to employ a normalization ($\mathbf{c}_0 = \mathbf{i}c_0$ and $\mathbf{c}_2 = \mathbf{i}c_2$), where the upper and lower partitions of $\mathbf{c}_0$ and $\mathbf{c}_2$ correspond to a magnetic component and a normalized electric component, respectively. These Fourier components are both continuous across any interlayer interface and form the basis for wave matching. Then, (27) is simplified to

$$\mathbf{c}_0 = \mathbf{d}_1\mathbf{b}_1^{-1}\mathbf{d}_1^{-1}\mathbf{c}_2 , \tag{28}$$

where the linear operators $\mathbf{d}_1 = \mathbf{d}\left(a_1, k_x^{-1}\gamma_1^{-1}a_1k_{x,1}\right)$ and $\mathbf{b}_1 = \mathbf{i}b_1\mathbf{i}^{-1}$ are unique for each layer with a given distribution of elementary materials (γ_1), defined matrices of the proper values $k_{x,1}$ and the proper vectors a_1.

For the trivial case of a uniform slab with a permittivity $\overline{\varepsilon}_1$, $a_1 = \mathrm{i}$, $\gamma_1 = \overline{\varepsilon}_1\mathrm{i}$ and a generalized analog of (6) is

$$\begin{pmatrix}\tilde{h}_0\\ \tilde{h}_0'\end{pmatrix} = \begin{pmatrix}\mathrm{i} & \mathrm{o}\\ \mathrm{o} & \eta_1\end{pmatrix}\mathbf{i}\begin{pmatrix}\beta_1^{-1} & \mathrm{o}\\ \mathrm{o} & \beta_1\end{pmatrix}\mathbf{i}^{-1}\begin{pmatrix}\mathrm{i} & \mathrm{o}\\ \mathrm{o} & \eta_1^{-1}\end{pmatrix}\begin{pmatrix}\tilde{h}_2\\ \tilde{h}_2'\end{pmatrix}, \tag{29}$$

where the tangential fields are the corresponding matrices of the Fourier transforms, $\tilde{h} = v^{-1}h$, $\tilde{h}' = (\iota kv)^{-1}h'$; $\eta_1 = diag\left(\overline{\varepsilon}_1^{-1}k_x^m\right)$ (from (24), $k_{x,1}^2 = \overline{\varepsilon}_1\mathrm{i} - k_y^2$, and $k_{x,1}^m = \sqrt{\overline{\varepsilon}_1 - \left(k_y^m\right)^2}$). Then for example, validation of (29) for a plane wave at normal incidence gives a familiar result, shown earlier in (11).

From (28) we also note that in general, the following identity holds

$$\begin{aligned}\begin{pmatrix}\tilde{h}_0\\ \tilde{h}_0'\end{pmatrix} &= \begin{pmatrix}a_1 & \mathrm{o}\\ \mathrm{o} & k_x^{-1}\gamma_1^{-1}a_1k_{x,1}\end{pmatrix}\\ &\times\begin{pmatrix}\cos k_{x,1}\delta_1 & -\iota\sin k_{x,1}\delta_1\\ -\iota\sin k_{x,1}\delta_1 & \cos k_{x,1}\delta_1\end{pmatrix}\\ &\times\begin{pmatrix}a_1^{-1} & \mathrm{o}\\ \mathrm{o} & k_{x,1}^{-1}a_1^{-1}\gamma_1k_x\end{pmatrix}\begin{pmatrix}\tilde{h}_2\\ \tilde{h}_2'\end{pmatrix},\end{aligned} \tag{30}$$

with $\cos k_{x,1}\delta_1$ and $\sin k_{x,1}\delta_1$ being arranged of adequate matrix exponentials.

II. SHA IN BI-PERIODIC NIM LAYERS

As yet there has been no mention of how to handle bi-periodic structures with generally different periods in z and y directions (denoted here as l_y and l_z respectively, as shown in Fig. 3). In contrast to the previous example, essentially there are two difficulties to overcome. First, there are a dramatically larger number of spatial harmonics ($\widehat{m}^2$ in bi-periodic structures, versus $\widehat{m}$ in the single-periodic NIMs of Fig. 2a). This volume could be quite demanding for pure numerical solvers. On top of that, the already large number of basis spatial

♦ i.e., a piecewise continuous function with a limited variation on *l*.

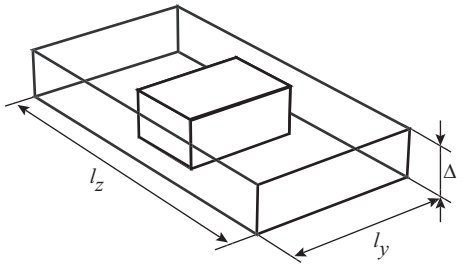

Fig. 3. Sketch of an example 3D periodic cell.

harmonics in which the fields is expressed should be increased even further to ensure convergence of the eigenvalues. A simple example of a bi-periodic layer of a binary material is shown in Fig. 3, where the layer is arranged of a metallic rectangular block which is immersed in a dielectric host. Certainly in real life applications each elementary layer (cross-section) could be much more involved. The electromagnetic field components inside a bi-periodic structure also should be bi-periodic with periods being the same as the length (l_y) and width (l_z) of the unit cell.

Then, each field component (e.g., $\vec{H} = \left(h_x, h_y, h_z\right)$) can be expressed as

$$h_i = \tilde{v}_i \tilde{u} c_i,\ i = x, y, z\,, \tag{31}$$

where each field component is written as the product of a cell periodic part $\tilde{v} = \tilde{v}(y,z)$ and a wavelike part $\tilde{u} = \exp(\iota \tilde{k}_x x)$, as a consequence of Bloch's theorem.

As usual, we start with Maxwell's equations $\nabla \times \vec{E} = \iota\omega\vec{B}$, $\nabla \times \vec{H} = -\iota\omega\vec{D}$, and since $\nabla \cdot \vec{H} = 0$, i.e. $\nabla \times \nabla \times \vec{H} = -\nabla^2 \vec{H}$, we arrive at

$$-\nabla^2 \vec{H} = \varepsilon_r^{-1} \nabla \varepsilon_r \times \left(\nabla \times \vec{H}\right) + k^2 \varepsilon_r \vec{H}\,. \tag{32}$$

Introducing a tangent field $\vec{h}_\tau = \hat{\mathbf{y}} h_y + \hat{\mathbf{z}} h_z$, we note that

$$-\nabla^2 \vec{h}_\tau = \omega^2 \varepsilon \mu \vec{h}_\tau + \varepsilon^{-1} \begin{pmatrix} \hat{\mathbf{y}} \partial_z \varepsilon \left(\partial_y h_z - \partial_z h_y\right) \\ -\hat{\mathbf{z}} \partial_y \varepsilon \left(\partial_y h_z - \partial_z h_y\right) \end{pmatrix}. \tag{33}$$

After splitting the components of $\vec{h}_\tau$, (33) yields

$$\begin{aligned} -\nabla^2 h_y &= \omega^2 \varepsilon \mu h_y + \varepsilon^{-1} \partial_z \varepsilon \left(\partial_y h_z - \partial_z h_y\right), \\ -\nabla^2 h_z &= \omega^2 \varepsilon \mu h_z + \varepsilon^{-1} \partial_y \varepsilon \left(\partial_z h_y - \partial_y h_z\right). \end{aligned} \tag{34}$$

Then, using separation of variables (31) in matrix form, $\vec{h}_\tau = \tilde{v}\tilde{u}\vec{c}$, where $\tilde{v} = \tilde{v}(x,y)$, $\tilde{u} = \tilde{u}(z)$, the above is rewritten as

$$\begin{aligned} \left(a_y k_x^2 a_y^{-1}\right) a_y \tilde{u} c_y &= \begin{pmatrix} v^{-1}\varepsilon v - \left(k_y^2 + k_z^2\right) \\ -\iota v^{-1}\varepsilon^{-1}\partial_z \varepsilon v k_z \end{pmatrix} a_y \tilde{u} c_y \\ &\quad + \iota v^{-1}\varepsilon^{-1}\partial_y \varepsilon v k_y a_z \tilde{u} c_z, \\ \left(a_z k_x^2 a_z^{-1}\right) a_z \tilde{u} c_z &= \begin{pmatrix} v^{-1}\varepsilon v - \left(k_y^2 + k_z^2\right) \\ -\iota v^{-1}\varepsilon_r^{-1}\partial_y \varepsilon_r v k_y \end{pmatrix} a_z \tilde{u} c_z \\ &\quad + \iota v^{-1}\varepsilon^{-1}\partial_y \varepsilon v k_z a_z \tilde{u} c_y, \end{aligned} \tag{35}$$

where

$k_z = \alpha_z \mathrm{i} + diag\left[m_z \lambda / l_z\right]$, $\quad k_y = \alpha_y \mathrm{i} + diag\left[m_y \lambda / l_y\right]$, $\alpha_y \hat{\mathbf{y}} + \alpha_z \hat{\mathbf{z}} = \vec{k}_0 - \left(\vec{k}_0 \cdot \hat{\mathbf{x}}\right)\hat{\mathbf{x}}$, and $\vec{k}_0 = \vec{k} / \left|\vec{k}\right|$ is a unit vector defined by the wavevector ($\vec{k}$) of the incident field.

The latter is further simplified with the aid of the following identities for the partial logarithmic derivatives

$$\begin{aligned} \iota v^{-1}\varepsilon^{-1}\partial_z \varepsilon v &= \gamma k_z \gamma^{-1} - k_z\,, \\ \iota v^{-1}\varepsilon^{-1}\partial_y \varepsilon v &= \gamma k_y \gamma^{-1} - k_y\,, \end{aligned} \tag{36}$$

where $\gamma = v^{-1}\varepsilon v$. Then we arrive at

$$\begin{aligned} \left(a_y k_x^2 a_y^{-1}\right) a_y \tilde{u} c_y &= \left(\gamma - k_y^2 - \gamma k_z \gamma^{-1} k_z\right) a_y \tilde{u} c_y \\ &\quad + \left(\gamma k_z \gamma^{-1} k_y - k_z k_y\right) a_z \tilde{u} c_z\ , \\ \left(a_z k_x^2 a_z^{-1}\right) a_z \tilde{u} c_z &= \left(\gamma k_y \gamma^{-1} k_z - k_y k_z\right) a_y \tilde{u} c_y \\ &\quad + \left(\gamma - k_z^2 - \gamma k_y \gamma^{-1} k_y\right) a_z \tilde{u} c_z. \end{aligned} \tag{37}$$

The second term in the right side of both equations in (37) corresponds to the cross polarization. For a symmetric grating we can show that both $\left(\gamma k_z \gamma^{-1} k_y - k_z k_y\right)$ and $\left(\gamma - k_z^2 - \gamma k_y \gamma^{-1} k_y\right)$ are equal to zero and consequently we have no cross polarization for symmetric gratings. This simplification yields two decoupled eigenvalue equations as shown below

$$\begin{aligned} a_y k_x^2 a_y^{-1} &= \gamma\left(\mathrm{i} - k_z \gamma^{-1} k_z\right) - k_y^2 \\ a_z k_x^2 a_z^{-1} &= \gamma\left(\mathrm{i} - k_y \gamma^{-1} k_y\right) - k_z^2. \end{aligned} \tag{38}$$

For an asymmetric grating the two eigenvalue equations would be coupled via the cross polarizations term.

A 2D TM case ($c_y = k_z = \mathrm{o}$, i.e. the structure is periodic in the *y* direction only, there is no magnetic field

along the direction of periodicity) gives ($\tilde{\gamma}_y = v^{-1}\varepsilon_r(y)v$)

$$a_z k_x^2 a_z^{-1} = \gamma_y\left(\mathrm{i} - k_y\gamma_y^{-1}k_y\right), \tag{39}$$

while a 2D TE case ($c_y = k_y = \mathrm{o}$, i.e. the structure is periodic in *z*-direction only, there is no electric field along the direction of periodicity and $\gamma_z = v^{-1}\varepsilon(z)v$) is

$$a_z k_x^2 a_z^{-1} = \gamma_z - k_z^2 . \tag{40}$$

Note that equations (39)-(40) also provide a solution for structures with interleaving single-period layers with 90-degree rotation of their periodicity directions.

III. CASCADING THE ELEMENTARY LAYERS

Cascading a set of q elementary layers (depicted in Fig. 2c) gives

$$c_0 = w_1 c_1 . \tag{41}$$

Here, $w_1 = \prod_{\nu=1}^{q}\tilde{w}_\nu$ and $\tilde{w}_\nu = s_\nu b_\nu^{-1}s_\nu^{-1}$ is an elementary transform due to ν-th layer.

Provided that each subset of q elementary layers is again stacked m times, then the matrix power $w_0^m = [w_0]^m$ is used with the following transformation

$$c_0 = w_0^m c_1 . \tag{42}$$

Transformations equivalent to (27) - (42) can be written as

$$\begin{pmatrix} c_i \\ c_r \end{pmatrix} = \begin{pmatrix} w_{0,0} & w_{0,1} \\ w_{1,0} & w_{1,1} \end{pmatrix}\begin{pmatrix} c_t \\ 0 \end{pmatrix}, \tag{43}$$

where c_i are the spatial harmonic coefficients of the source, c_r is a set of the spatial harmonic coefficients of reflected light, and c_t are the harmonic coefficients of transmitted light.

A. Reflection and Transmission Coefficients

The major work-load in the above method falls on the calculation of the proper values and vectors ($k_{x,\nu}$ and a_ν) for each elementary layer. Once the values are obtained, the characteristic matrices of each layer are arranged as $s_\nu b_\nu^{-1}s_\nu^{-1}$.

Introducing the transformations $\rho_\nu c_{t,\nu} = c_{r,\nu}$, $\tau_\nu c_{t,\nu} = c_{t,q}$ (with initial values given by $\tau_q = \mathrm{i}$, and $\rho_q = \mathrm{o}$), the matrices of spatial spectral reflectance and transmittance are defined as

$$\begin{aligned} \rho_{\nu-1} &= \left(w_\nu^{1,0} + w_\nu^{1,1}\rho_\nu\right)\left(w_\nu^{0,0} + w_\nu^{0,1}\rho_\nu\right)^{-1}, \\ \tau_{\nu-1} &= \tau_\nu\left(w_\nu^{0,0} + w_\nu^{0,1}\rho_\nu\right)^{-1}, \end{aligned} \tag{44}$$

where the characteristic matrix is partitioned as $\tilde{w}_\nu = \left(\begin{array}{c|c} w_\nu^{0,0} & w_\nu^{0,1} \\ \hline w_\nu^{1,0} & w_\nu^{1,1} \end{array}\right)$. The partitions are calculated using s_ν, which is a matrix with symmetrical partitions, $s_\nu = \mathrm{s}\left(s_\nu^0, s_\nu^1\right)$ with $s_\nu^0 = \frac{1}{2}\left(k_x^{-1}\gamma_\nu^{-1}a_\nu k_{x,\nu} + a_\nu\right)$ and $s_\nu^1 = \frac{1}{2}\left(k_x^{-1}\gamma_\nu^{-1}a_\nu k_{x,\nu} - a_\nu\right)$ and a similar matrix $s_\nu^{-1} = \mathrm{s}\left(\tilde{s}_\nu^0, \tilde{s}_\nu^1\right)$ with $\tilde{s}_\nu^0 = \frac{1}{2}\left(k_{x,\nu}^{-1}a_\nu^{-1}\gamma_\nu k_x + a_\nu^{-1}\right)$ and $\tilde{s}_\nu^1 = \frac{1}{2}\left(k_{x,\nu}^{-1}a_\nu^{-1}\gamma_\nu k_x - a_\nu^{-1}\right)$, then

$$\begin{aligned} &w_\nu^{0,0} = s_\nu^0\beta_\nu^{-1}\tilde{s}_\nu^0 + s_\nu^1\beta_\nu\tilde{s}_\nu^1,\ w_\nu^{0,1} = s_\nu^0\beta_\nu^{-1}\tilde{s}_\nu^1 + s_\nu^1\beta_\nu\tilde{s}_\nu^0, \\ &w_\nu^{1,0} = s_\nu^1\beta_\nu^{-1}\tilde{s}_\nu^0 + s_\nu^0\beta_\nu\tilde{s}_\nu^1,\ w_\nu^{1,1} = s_\nu^1\beta_\nu^{-1}\tilde{s}_\nu^1 + s_\nu^0\beta_\nu\tilde{s}_\nu^0 . \end{aligned} \tag{45}$$

Thus, for example, a single-layer structure is calculated as follows: $\tau_0 = \left(w_1^{0,0}\right)^{-1}$, $\rho_0 = w_1^{1,0}\left(w_1^{0,0}\right)^{-1}$. Then, the transmitted and reflected Bloch-Floquet waves are

$$c_{t,1} = \tau_0 c_i ,\ c_{r,0} = \rho_0 c_i . \tag{46}$$

B. A Simple Validation Test

A simplified 2D single-layer model for validating the simulation method is shown in Fig. 4a. The sample structure is intentionally made of a very thin metallic grating (with 10-nm thickness). The grating is arranged of 400-nm gold strips separated by narrow strips of silica, the period of the structure is 480 nm. The large aspect ratio of the metallic strips and a large electric resonance at a wavelength of about 1.2 micron are among the main challenges of the test model. To obtain a good set of reference data, the structure was simulated using a commercial software package with 5$^{\text{th}}$-order finite elements. The validity of the FEM solution was verified by using the same model with different levels of additional meshing refinement and an adaptive solver. The results were stable upon the use of 41,000 degrees of freedom (field variables), where the bulk of the resources had been spent for the free-space buffer, non-reflecting lay-

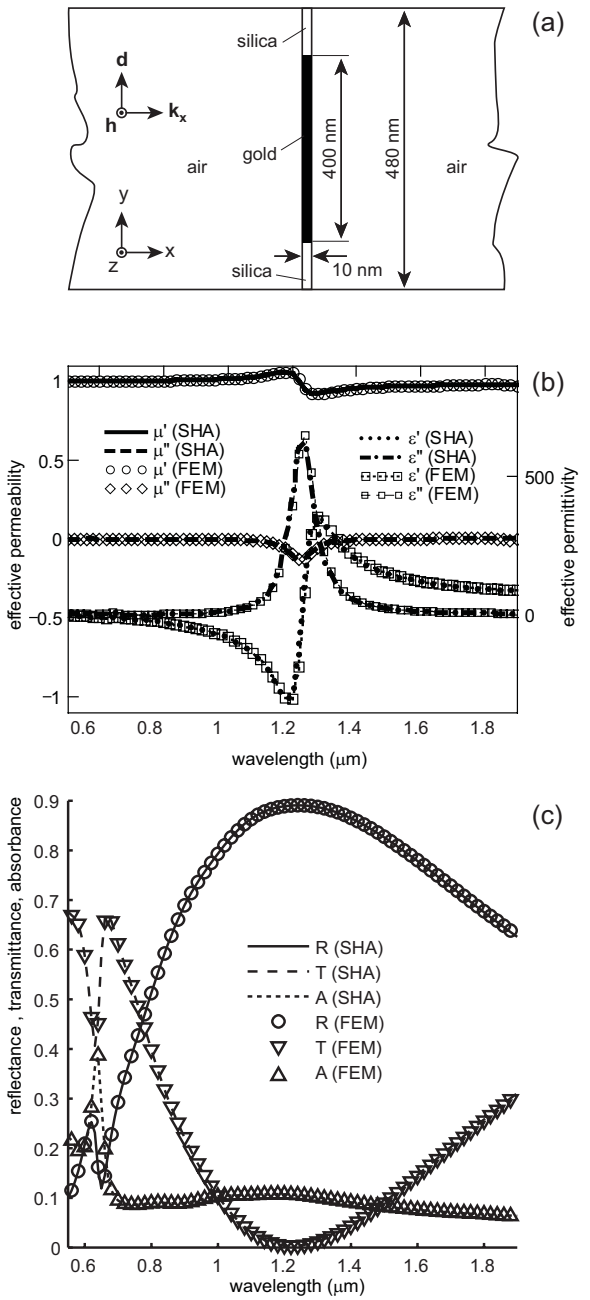

Fig. 4. (a) Geometry sketch of a resonant elementary layer; (b) effective permeability and permittivity obtained for the elementary layer using FEM and SHA (using 11 eigenvalues); (c) comparison of the reflection, transmission, and absorption spectra obtained in simulations using FEM and SHA (11 eigenvalues).

ers and adequate meshing at the corners.

In contrast to FEM, the spatial harmonic analysis method appeared much more efficient. The problem was stabilized after the use of 11 eigenvalues with a calculation time of about 100 times less versus the FEM solver with the same number of wavelength points and the same computational hardware. It should be noted that the amount of simulation time using SHA is approximately proportional to the total number of elementary layers and scales approximately as the square (or cube) of the total number of eigenvalues in 2D (or 3D) problems, while the performance of FEM solvers decreases very moderately with increasing layers. Both models appeared to be quite sensitive to the material properties of the metal. In both cases, the interpolated complex refractive index was based on the experimental table of Johnson and Christy [19]. In addition to simple validation of the modeling approach, the test model of Fig. 4a reveals all typical features of the periodic structures with localized plasmonic resonances, e.g. at the same wavelength the electric resonance is always accompanied by a satellite magnetic antiresonance and vise versa.

As has been discussed in [5] and shown in equations (10) and (11), the effective refractive index $\overline{n}_1$ and its effective impedance $\overline{\eta}_1$ of a given elementary layer can be uniquely determined either experimentally or from simulations. Rewriting (10) as

$$\overline{n}_1 = \frac{1}{\delta_1}\left(\begin{array}{l}\arccos\dfrac{1-\overline{r}^2+n_2\overline{t}^2}{\left[1+n_s-(1-n_2)\overline{r}\right]\overline{t}} \\ +2\pi\delta_1\nu\end{array}\right), \qquad \nu = 0,1,2\ldots \tag{47}$$

we can determine $\overline{n}_1$, where n_2 is the refractive index of the thick substrate beyond the elementary layer, and $\overline{r}$ and $\overline{t}$ are the complex reflection and transmission coefficients of the propagating plane wave mode. In simulations $\overline{r}$ and $\overline{t}$ can be obtained from

$$\overline{t} = \left(\tau_0\right)_{0,0},\ \overline{r} = \left(\rho_0\right)_{0,0}, \tag{48}$$

i.e., in essence by taking only the central terms of the transmission and reflection matrices. Then, the effective permittivity and the effective permeability are given by

$$\overline{\mu}_1 = \overline{n}_1\overline{\eta}_1,\ \overline{\varepsilon}_1 = \overline{n}_1/\overline{\eta}_1\,. \tag{49}$$

C. Implementation Details for the 2D Case

Although the process of solving (24) is relatively simple for dielectric sub-wavelength gratings, a direct treatment of metallic sub-wavelength gratings is more difficult because of the much higher contrast in permittivity within the optical wavelength range.

The following steps are taken to alleviate the problem:

1) The Fourier transform of inverted permittivity

First, we take the following modification of (23)

$$k^2 h_1 + \varepsilon_1^{-1}\partial_x^2 h_1 + \partial_y\left(\varepsilon_1^{-1}\partial_y h_1\right) = 0\,. \tag{50}$$

Using $h_1 = v a_1\left(u_1 c_{t,1} - u_1^{-1} c_{r,1}\right)$ and $\varepsilon_1^{-1} = v\tilde{\gamma}_1 v^{-1}$ we have

$$v - v\tilde{\gamma}_1 a_1 k_{x,1}^2 a_1^{-1} + \left(\partial_y v\right)\imath\tilde{\gamma}_1 k_x = 0\,, \tag{51}$$

or

$$\mathrm{i} - k_y\tilde{\gamma}_1 k_y = \tilde{\gamma}_1 a_1 k_x^2 a_1^{-1}\,. \tag{52}$$

Finally, we can use the following version of (24)

$$a_1 k_{x,1}^2 a_1^{-1} = \tilde{\gamma}_1^{-1}\left(\mathrm{i} - k_y\tilde{\gamma}_1 k_y\right), \tag{53}$$

which provides stable convergence in the presence of metallic elements.

Moreover, in accord with (53) the Fourier transform of the inverted permittivity $\tilde{\gamma}_1$ and its inverse $\tilde{\gamma}_1^{-1}$ is used respectively in (28) and (30) instead of γ_1^{-1} and γ_1.

2) Analytical calculation of the Fourier transform

In addition, along with the use of the inverted permittivity, the Fourier transformation $\tilde{\gamma}_1$ in (25) is calculated analytically provided that $\varepsilon_1(y)$ over the period l is a combination of homogeneous segments. Indeed, for any $m > 0$ $l^{-1}\int e^{-\imath k k_y^m y} dy = e^{-\imath k k_y^m y}\Big/\left(l k k_y^m\right)$, thus for example, a term $\tilde{\gamma}_1^{p,m}$ (at row p and column m) of the square matrix $\tilde{\gamma}_1$ for the elementary layer in Fig. 4a, is given by

$$\begin{matrix}\left(\varepsilon_g^{-1} + \varepsilon_s^{-1}\right)\dfrac{\sin\left[\kappa\pi(p-m)\right]}{\pi(p-m)} & if\ p \neq m \\ \kappa\varepsilon_g^{-1} + (1-\kappa)\varepsilon_s^{-1} & otherwise\end{matrix}, \tag{54}$$

where $\kappa = w/l$ is the metal filling factor and ε_g and ε_s is the permittivity of gold and silica, respectively.

IV. DISCUSSIONS

Both remedies built on (53) and (54) work well with metallic structures. For example, Fig. 5 shows the real and imaginary parts of the effective refractive index that is restored using the complex transmission and reflection coefficients at normal incidence [5]. (The geometry of the layer has been already shown in Fig. 4a.) Both real and imaginary parts of the refractive index are converging rapidly. Small features around 650 nm are suppressed only for $m_{\max} = 1$, and both curves are quickly converging to their limits; starting from $m_{\max} = 9$ the corresponding curves with larger $m_{\max}$ are overlapping.

In contrast, a direct application of the initial formulation (24) is of limited utility to the problem. We note that the transmission and reflection spectra demonstrate much slower convergence and substantial artifacts. For example, Fig. 6 depicts the results obtained from the problem of Fig. 4a using the initial eigenvalue formulation (24).

It is important to note that a convergence control should be implemented for the entire multilayer structure; otherwise insignificant modes of an elementary layer could be considerably enhanced due to additional resonances of coupled elementary layers.

Consider for example the real part of the refractive index, n', shown in Fig. 7a. The values of n' are restored from $\overline{r}$ and $\overline{t}$, which are calculated for a single

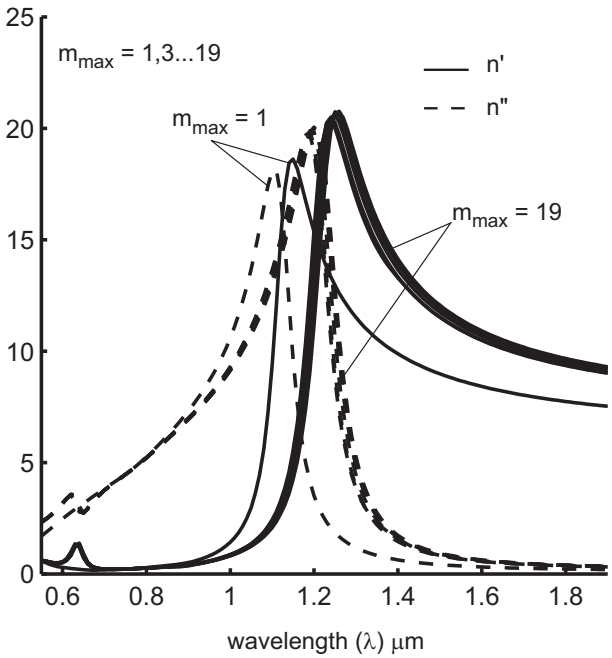

Fig. 5. Real and imaginary part of the refractive index (n' and n'') vs. wavelength calculated with a different number of spatial harmonics ($m_{\max}$ = 1, 3, 19). Starting from $m_{\max}$ = 9 the difference in the results is almost indiscernible.

layer depicted in the inset of Fig. 7a. There is no resonance within the selected 300-nm wavelength segment,

and the values of n' converge quickly starting from $m_{\max} = 6$.

Now we take a triple-layer structure arranged of two identical elementary layers of Fig. 7a separated by a uniform 100-nm layer of silica. The structure exhibits an additional magnetic resonance within the selected wavelength range. As expected, this resonance, which appears due to additional near-field coupling between the metallic strips, requires taking into account an increased number of modes. The same level of relative error is now achieved starting from $m_{\max} > 10$.

As a result, additional care is required for the accurate calculation of stacked substructures arranged of elementary layers and cascaded materials integrating different or identical multilayer substructures. It also follows from the analysis of equations (27)-(45) that:

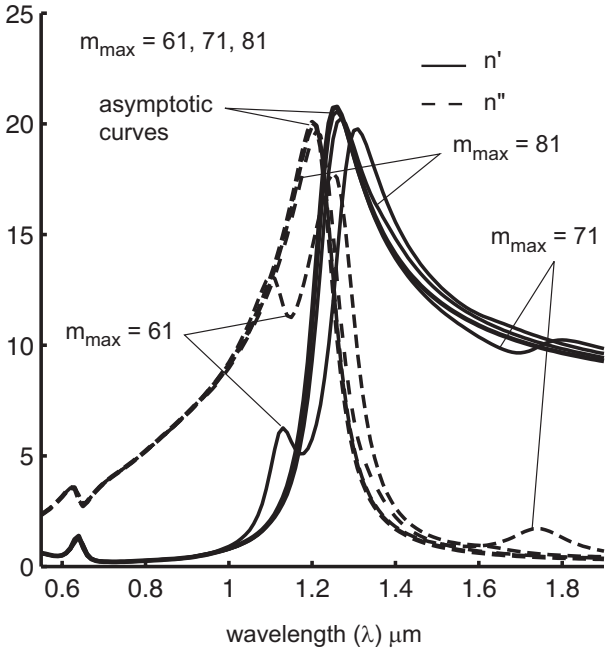

Fig. 6. Real and imaginary part of the refractive index (n' and n'') vs. wavelength calculated using (24) for $m_{\max}$ = 61, 71, 81. Starting only from $m_{\max}$ = 71 the difference in the results are converging well to the asymptotic curves obtained using (53).

(i) None of asymmetric multilayer composites can be effectively described either by the simplified homogenization approach (9)-(11), or through its generalized analog (30). (A multilayer composite is asymmetric if it contains an odd number of elementary layers and the layers are not mirror-symmetric relative to the central layer; all structures with an even number of distinct layers are always asymmetric).

(ii) Effective optical parameters (including an effective negative refractive index) obtained in a single symmetric sub-set of elementary layers may not guarantee the same effective parameters in a bulk material arranged of identical subsets, not merely because of absorptive losses but also due to new interactions of near-field waves introduced by the use of cascading.

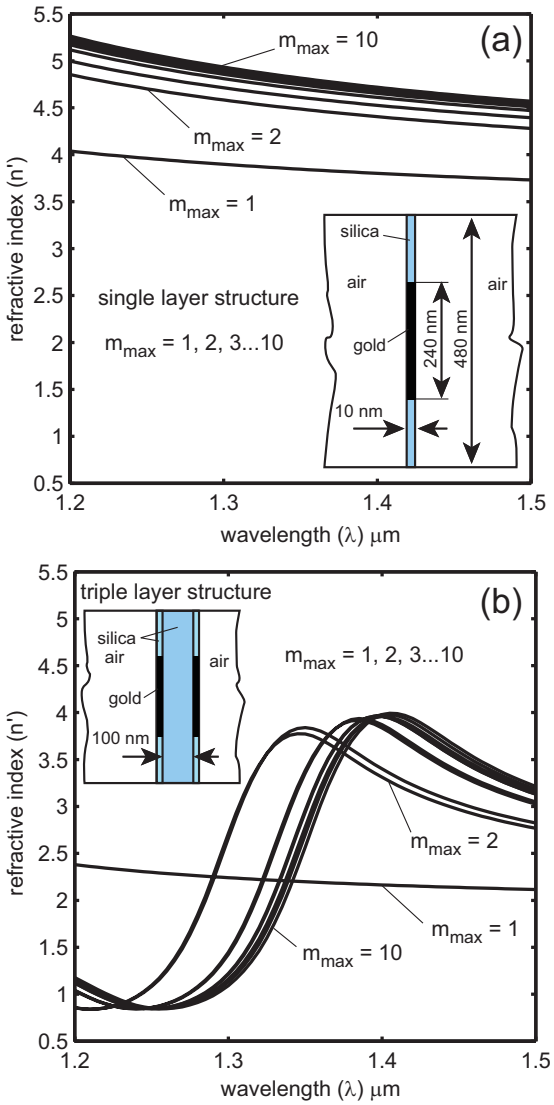

Fig. 7. The real part of the refractive index (n') vs. wavelength. (a) n' calculated for a single layer structure shown in the inset for $m_{\max}$ = 1, 2 ...10. Starting from $m_{\max}$ = 6 there is almost no difference in the curves, (b) n' calculated for a triple layer structure arranged from two identical layers of diagram (a) separated by a 100-nm uniform layer of silica. The inset depicts the triple-layer structure. Convergence to the same lever of error begins starting from $m_{\max}$ = 10. Slower convergence is caused by an additional resonance due to strong near-field coupling between the layers.

To illustrate (i) consider a classical example of a subset structure with two homogeneous lossless layers [[20], p. 72]. The characteristic matrix of two layers with thicknesses Δ_1 and Δ_2, and indices n_1 and η_1, is computed as $\mathbf{w}_2 = \tilde{\mathbf{w}}_1\tilde{\mathbf{w}}_2$, with $\tilde{\mathbf{w}}_1 = \mathbf{d}_1\mathbf{b}_1^{-1}\mathbf{d}_1^{-1}$ and $\tilde{\mathbf{w}}_2 = \mathbf{d}_2\mathbf{b}_2^{-1}\mathbf{d}_2^{-1}$. The effective characteristic matrix ($\mathbf{w}_{eff}$) of an equivalent single layer, which is defined as

$$\mathbf{w}_{eff} = \left(\begin{array}{c|c} \mathbf{w}_{eff}^{0,0} & \mathbf{w}_{eff}^{0,1} \\ \hline \mathbf{w}_{eff}^{1,0} & \mathbf{w}_{eff}^{1,1} \end{array}\right) = \begin{pmatrix} \cos n_{eff}k_x\delta & -\imath n_{eff}\sin n_{eff}k_x\delta \\ -\imath n_{eff}^{-1}\sin n_{eff}k_x\delta & \cos n_{eff}k_x\delta \end{pmatrix}, \quad (55)$$

(using a scaled thickness, $\delta = k(\Delta_1 + \Delta_2)$ and the effective index, n_{eff}), should be equal to the characteristic matrix of the double-layer $\mathbf{w}_2$. To be equivalent to $\mathbf{w}_{eff}$, the product $\mathbf{w}_2 = \tilde{\mathbf{w}}_1\tilde{\mathbf{w}}_2$ must have identical diagonal partitions since $\mathbf{w}_{eff}^{0,0} = \mathbf{w}_{eff}^{1,1}$ in (55). This is true only if the product commutes, i.e. $\tilde{\mathbf{w}}_1\tilde{\mathbf{w}}_2 = \tilde{\mathbf{w}}_2\tilde{\mathbf{w}}_1$, leaving the only trivial case of $n_1 = n_2$ possible. Therefore, even a simple stack of two distinct lossless films cannot be adequately modeled by a single effective layer. Physically, the condition $\tilde{\mathbf{w}}_1\tilde{\mathbf{w}}_2 = \tilde{\mathbf{w}}_2\tilde{\mathbf{w}}_1$ means that the effective parameters of a multilayer NIM should not depend on which side is chosen for illumination, i.e. its structure should be symmetric.

Note that although $\tilde{\mathbf{w}}_1\tilde{\mathbf{w}}_2\tilde{\mathbf{w}}_3 = \tilde{\mathbf{w}}_3\tilde{\mathbf{w}}_2\tilde{\mathbf{w}}_1$ is always true for any triple-layered structure, since the first and the last layers are equal ($\tilde{\mathbf{w}}_1 = \tilde{\mathbf{w}}_3$), the homogenization of $\mathbf{w}_3 = \mathbf{d}_1\left(\mathbf{b}_1^{-1}\mathbf{d}_{12}\mathbf{b}_2^{-1}\mathbf{d}_{12}^{-1}\mathbf{b}_1^{-1}\right)\mathbf{d}_1^{-1}$ is not very simple even for the structure with homogeneous elementary layers.

Now to exemplify (ii) consider a cascaded structure arranged of identical symmetric substructures, then $w_3 = s_1b_1^{-1}s_{12}b_2^{-1}s_{12}^{-1}b_1^{-1}s_1^{-1}$, where $s_{12} = s_1^{-1}s_2 = \mathbf{i}^{-1}\mathbf{d}_1^{-1}\mathbf{d}_2\mathbf{i}$. The diagonally partitioned matrix $\mathbf{d}_1^{-1}\mathbf{d}_2$ is responsible for interactions between the layers. Cascading p triple-layer substructures suggests taking the p-th power of the characteristic matrix w_3. Although the result is straightforward since $(w_3)^p = s_1\left(b_1^{-1}s_{12}b_2^{-1}s_{12}^{-1}b_1^{-1}\right)^p s_1^{-1}$, it is clear that new interactions of near-field waves introduced by cascading will change the effective properties of the cascaded structure in comparison to those of the initial three-layer sub-structure, unless it is possible to write w_3 as $w_3 = s_{eff}b_{eff}s_{eff}^{-1}$, where b_{eff} is a diagonal matrix of effective eigenvalues and s_{eff} is a matrix of effective eigenvectors.

ACKNOWLEDGMENT

We would like to cite fruitful teamwork with V. Drachev, T. Klar, V. Shalaev, W. Cai, Z. Liu, and H.-K. Yuan. The authors also acknowledge important discussions with D. Werner.

This work was supported in part by ARO grant W911NF-04-1-0350, NSF-NIRT award ECS-0210445 and ARO MURI grant.

REFERENCES

[1] L. I. Mandel'shtam, "Group velocity in crystal lattice," *JETP*, vol. 15, pp. 475, 1945.

[2] V. G. Veselago, "The electrodynamics of substances with simultaneously negative values of ε and μ," *Soviet Physics Uspekhi*, vol. 10, pp. 509–514, 1968.

[3] R. A. Shelby, D. R. Smith, and S. Schultz, "Experimental verification of a negative index of refraction," *Science*, vol. 292, pp. 77–79, Apr. 2001.

[4] J. B. Pendry, "Negative refraction makes a perfect lens," *Phys. Rev. Lett.*, vol. 85, no. 18, pp. 3966–3969, Oct. 2000.

[5] A. V. Kildishev, W. Cai, U. K. Chettiar, H. K. Yuan, A. K. Sarychev, V. P. Drachev, and V. M. Shalaev, "Negative refractive index in optics of metal-dielectric composites," *J. of Opt. Soc. Am. B*, vol. 23, no. 3, pp. 423–433, Mar. 2006.

[6] J. D. Vacchione and R. Mittra, "Cascading of Multiscreen Frequency Selective Surfaces," in *Frequency Selective Surface and Grid Array*, T. K. Wu, Ed. John Wiley & Sons, 1995.

[7] C. B. Burkhardt, "Diffraction of a Plane Wave at a Sinusoidally Stratified Dielectric Grating," *J. Opt. Soc. Am.*, vol. 56, no. 11, pp. 1502–1509, Nov. 1966.

[8] F. G. Kaspar, "Diffraction by thick, periodically stratified gratings with complex dielectric constant", *J. Opt. Soc. Am.*, vol. 63, no. 1, pp. 37–45, Jan. 1973.

[9] K. Knop, "Rigorous diffraction theory for transmission phase gratings with deep rectangular grooves," *J. Opt. Soc. Am.*, vol. 68, no. 9, pp. 1206–1210, Sept. 1978.

[10] M. G. Moharam and T. K. Gaylord, "Rigorous coupled-wave analysis of planar-grating diffraction," *J. Opt. Soc. Am.*, vol. 71, no. 7, pp. 811–818, July 1981.

[11] M. G. Moharam and T. K. Gaylord, "Rigorous coupled-wave analysis of grating diffraction – E-mode

polarization and losses," *J. Opt. Soc. Am.*, vol. 73, no. 4, pp. 451–455, Apr. 1983.
[12] M. G. Moharam and T. K. Gaylord, "Three-dimensional vector coupled-wave analysis of planar-grating diffraction," *J. Opt. Soc. Am.*, vol. 73, no. 9, pp. 1105–1112, Sept. 1983.
[13] L. C. Botten, M. S. Craig, R. C. McPhedran, J. L. Adams, and J. R. Andrewartha, "The dielectric lamellar diffraction grating," *Opt. Acta,* vol. 28, no. 3, pp. 413–428, 1981.
[14] L. C. Botten, M. S. Craig, R. C. McPhedran, J. L. Adams, and J. R. Andrewartha, "The finitely conducting lamellar diffraction grating," *Opt. Acta*, vol. 28, no. 8, pp. 1087–1102, 1981.
[15] L. C. Botten, M. S. Craig, and R. C. McPhedran, "Highly conducting lamellar diffraction gratings," *Opt. Acta*, vol. 28, no. 8, pp. 1103–1106, 1981.
[16] G. Tayeb and R. Petit, "On the numerical study of deep conducting lamellar diffraction gratings," *Optica Acta*, vol. 31, no. 12, pp. 1361-1365, 1984.
[17] R. Petit and G. Tayeb, "Numerical study of the symmetrical strip-grating-loaded slab," *J. Opt. Soc. Am. A*, vol. 7, no. 3, pp. 373-378, Mar. 1990.
[18] S. E. Sandström, G. Tayeb, and R. Petit, "Lossy multistep lamellar gratings in conical diffraction mountings – an exact eigenfunction solution," *J. of Electromagnetic Waves and Applications*, vol. 7, pp. 631–649, 1993.
[19] P. Johnson and R. W. Christy, "Optical Constants of the Noble Metals," *Phys. Rev. B*, vol. 6, no. 12, pp. 4370–4379, Dec. 1972.
[20] M. Born and E. Wolf, *Principles of Optics*, Cambridge, 1964.

Alex V. Kildishev received the M.Sc., and Ph.D. degrees in electrical engineering from the Kharkov State Polytechnical University in the Ukraine. He has worked as a Senior Scientist at the Institute of Electrodynamics, Academy of Sciences, Ukraine. Since 1998 he has been a member of the School of ECE, Purdue University, where he is currently a Principal Research Scientist at the PSL, Birk Nano-technology Center. His primary research interest is in the development of advanced computational methods for the spatial harmonic/modal analysis in general radiation and scattering problems in applied electromagnetics and optics. Other research interests include optimization of plasmonic metamaterials, MRI electromagnetics, and magnetic silencing. He has published over sixty journal articles in these areas; he is a coauthor of four book chapters and four patents. Dr. Kildishev is a Senior Member of the IEEE, and is a member of ACES and ICS.

Uday K. Chettiar received a bachelor degree in electrical engineering from Indian Institute of Technology, Mumbai, India in 2003. He is currently working towards his Ph.D. degree at Prof. Shalaev's Photonics and Spectroscopy Laboratory (PSL), Purdue University, USA. He was a gold medalist in the Indian National Physics Olympiad and a recipient of Benjamin Franklin-Meissner fellowship at Purdue. He has published four papers in peer-reviewed journals and has given four talks at international scientific conferences. Uday Chettiar is a member of OSA. His current research interests include simulation and analysis of optical metamaterials.